



ChemComm

**Chemical Self-Assembly Strategies for Designing Molecular
Electronic Circuits**

Journal:	<i>ChemComm</i>
Manuscript ID	CC-COM-09-2019-007200.R1
Article Type:	Communication

SCHOLARONE™
Manuscripts

COMMUNICATION

Chemical Self-Assembly Strategies for Designing Molecular Electronic Circuits

Dustin Olson^a, Alejandro Boscoboinik^a and Wilfred T Tysoe^{*a}

Received 00th January 20xx,
Accepted 00th January 20xx

DOI: 10.1039/x0xx00000x

Design principles are demonstrated for fabricating molecular electronic circuits using the inherently self-limiting growth of molecular wires between gold nanoparticles from the oligomerization of 1,4-phenylene diisocyanide.

It is a significant experimental challenge to devise self-assembly strategies for the targeted design of electronic circuits based on molecules.¹⁻³ We recently proposed a self-limiting self-assembly method for selectively making controlled electrical connections between gold nano-electrode nodes⁴ based on the oligomerization of 1,4-phenylene diisocyanide (1,4-PDI), thereby eliminating the sensitivity of the interparticle linking process to the reactant dose.⁵ 1,4-PDI self-assembles on gold to form conductive, one-dimensional, oligomeric chains that comprise alternating gold and 1,4-PDI units⁶⁻¹⁰ in which a gold adatom is linked to two trans isocyanide groups. The self-limiting kinetics have been modelled using an oligomerization mechanism derived from density functional theory (DFT) calculations, which showed that oligomer growth is initiated by a vertical, mobile Au–1,4-PDI adatom complex that forms by binding to the gold substrate, which oligomerizes by the gold adatom attaching to the isocyanide terminus of a growing chain.¹¹ The DFT calculations also determined the activation barriers for the various elementary-step processes and showed that the diffusion barrier for the motion of the Au–1,4-PDI adatom complex was low, while the activation energy for oligomerization was found to be ~ 152 kJ/mol. A kinetic Monte Carlo analysis demonstrated that the extent of oligomerization was limited because both the formation of the mobile Au–1,4-PDI adatom complex and the propagation of the oligomer chain take place at the peripheral sites on the gold nanoparticle. As a result, the initiation and growth of oligomer chains eventually block the sites at which the Au–1,4-PDI adatom complexes are formed, thereby quenching the reaction to prevent the growth of further oligomers, and is therefore inherently self-limiting.⁴ Using the kinetic parameters found for the formation of oligomers on Au(111), the model predicted that the oligomers should be able to bridge gold nanoparticle nodes that were less than ~ 10 nm apart. It has previously been demonstrated that 1,4-PDI, and analogous molecules comprising two terminal anchoring –SH groups, can form conductive molecular bridges between adjacent

nanoparticles deposited onto an insulating mica substrate.^{9, 12-15} Oligomer-linked gold nanoparticles have been directly imaged using scanning tunnelling microscopy (STM)⁹ and 1,4-PDI and analogous dithiols have been used in single-molecule conductivity experiments.^{13, 14, 16-34} While the experiments on an insulating mica substrate did not measure the conductivity as a function of particle separation, they do demonstrate the ability of these bifunctional molecules to link between nanoparticles on surfaces.

The following work tests the prediction that the formation of conductive linkages between gold nanoparticles on an insulating silica support is self-limiting by measuring the conductivity of a relatively large array (~ 0.25 mm between the gold electrodes) of gold nanoparticles deposited by evaporating gold onto a silica substrate in high vacuum as a function of gold film thickness. While this approach did not lead to nanoparticle spacings as large as the limiting value of ~ 10 nm predicted by kinetic Monte Carlo simulations, it reveals a decrease in the change in conductivity after dosing with 1,4-PDI as the average gold nanoparticle spacing increased.

The ability to bridge nanogaps was therefore explored in greater detail using devices consisting of lithographically fabricated nanoelectrodes with gap spacings of ~ 30 nm, significantly larger than the limiting spacing predicted from kinetic Monte Carlo simulations. They showed no conductivity after dosing with 1,4-PDI. Hybrid devices were also fabricated by evaporating a thin film of gold on the

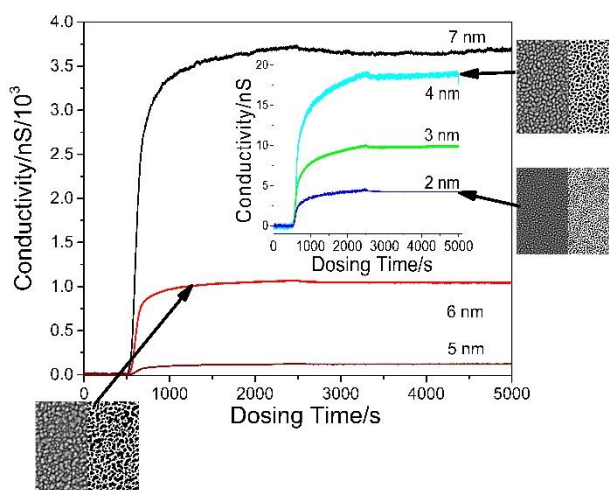


Fig. 1: Plot of conductivity change versus 1,4-PDI dosing time, where dosing was initiated at $t = 500$ s at a background pressure of 1×10^{-8} Torr at a sample temperature of 280 K for various thicknesses of gold evaporated into a silica substrate, where the film thicknesses are indicated.

^a Department of Chemistry and Biochemistry and Laboratory for Surface Studies, University of Wisconsin-Milwaukee, Milwaukee, WI 53211, USA.

Electronic Supplementary Information (ESI) available: Fig. S1, temperature dependence of 1,4-PDI-covered nanoparticle array; Figs. S2 to S4, estimates of interparticle separation as a function of film thickness. See DOI: 10.1039/x0xx00000x

COMMUNICATION

ChemComm

nanoelectrode devices in vacuo to introduce nanoparticles in the interelectrode region to reduce the gap.³⁵ These hybrid devices displayed significant electron conductivity thereby experimentally verifying the postulate discussed above.⁴

The results of experiments carried out on thin gold films deposited between gold contacts separated by ~ 0.25 mm are shown in Figure 1 as a function of film thickness, where it is expected that the separation between nanoparticles will decrease as the thickness of the gold film increases. The samples were then exposed to a constant flux of 1,4-PDI and the conductivity of the samples monitored as a function of time. In all cases, the conductivity rises with increasing 1,4-PDI dose to reach a saturation conductivity that depends on the thickness of the initial gold film (Fig. 1). All samples showed a variation in conductivity with temperature and a typical plot of the temperature dependence for a 6.5 nm thick gold film is shown in Fig. S1 ESI[†], where $\ln(\sigma)$ varies as $1/\sqrt{T}$, where σ is the conductivity of the sample and T is the absolute temperature. This behaviour has been observed for arrays of gold nanoparticles deposited onto mica^{9, 12, 15, 36} and is typical for electron transport through disordered nanoparticle arrays.³⁷⁻⁴¹ The conductivity between linked nanoparticles comprises an electron tunnelling term that varies as $\sim \exp(-\beta L)$ where L is the length of the molecular linkage between gold nodes, and β is a decay parameter,^{42, 43} which is independent of temperature, and a Coulomb charging energy term, which varies as $\sim \exp(-\frac{E_C}{k_B T})$ where E_C is the Coulomb charging energy, k_B is the Boltzmann constant and T is the absolute temperature, and combine to lead to the experimentally observed temperature dependence.⁴¹

The initial and final conductivities of the gold nanoparticle arrays before and after saturating with 1,4-PDI are displayed in Figure 2 as a function of the thickness of the gold film. SEM images of the gold film were analysed to estimate the average interparticle spacing as a function of film thickness (See ESI[†] for an outline of the analysis) and the ratio of the final to initial conductivities are plotted versus the estimated interparticle separations in the inset in Figure 2, where the

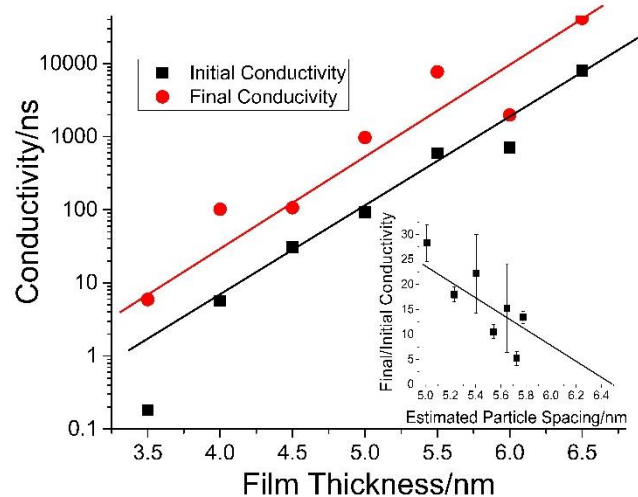


Fig. 2: Plot of the initial conductivity for an array of nanoparticles grown by gold evaporation onto a silica support in high vacuum where the values are shown before (■) and after (●) saturating the sample with 1,4-PDI as a function of the thickness of the gold film. Shown as an inset are the ratios of the final to the initial conductivities plotted versus the estimated particle separation.

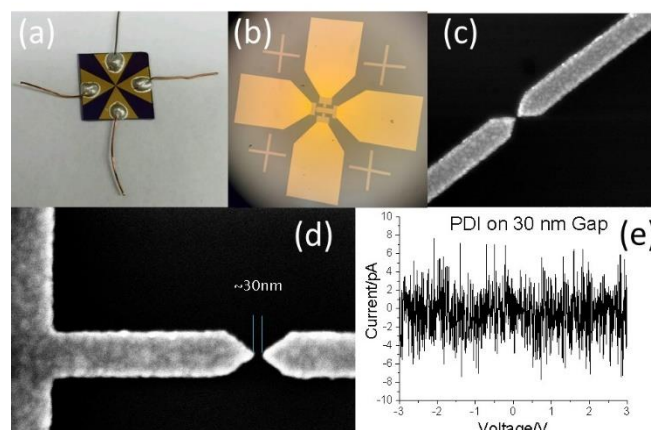


Fig. 3: Depiction of the gold nanogaps grown on silica. (a) shows the wiring of the electrode to the connection pads, (b) shows the connecting pads and the nanoelectrodes, (c) shows a high-resolution SEM images of the gold nanogaps, and (e) displays an I/V curve after dosing with 1,4-PDI.

conductivity ratios are plotted to take into account the different percolation pathways on the films with different gold thicknesses. Extrapolating this line shows that the ratio becomes unity at an interparticle separation of 7 ± 2 nm, indicating that the bridging of initially separated gold nanoparticles by conducting 1,4-PDI–Au oligomers is indeed self-limiting.

In order to confirm this, and to more accurately estimate the limiting distance, experiments were carried out using a 30-nm nanogap between gold electrodes as depicted in Figure 3. The design of the nanogaps is shown in Figs. 3 (a) to (d), where Fig. 3(d) shows that the gap separation is ~ 30 nm. The sample was then saturated with 1,4-PDI and the I/V curve measured (Figure 3(e)). This shows no conductivity between the electrodes within the detection sensitivity. To determine whether decreasing the gap size leads to bridging by conductive 1,4-PDI–Au oligomers, hybrid devices were fabricated by evaporating a thin film of gold onto the nanogap devices in vacuo. Two types of structure observed. The first, shown in Figure 4(a)

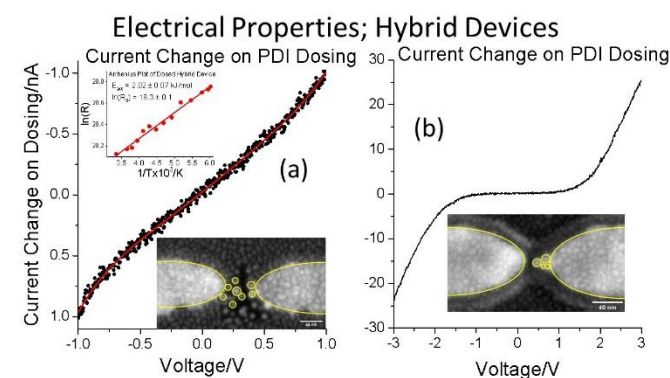


Fig. 4: (a) Plot of the change in the I/V curve for the 1,4-PDI-saturated hybrid device (shown as an Inset, where the images are 300 nm across), where the gold nanoelectrodes and the gold nanoparticles within the gap are highlighted in yellow. The inset to Figure (a) shows a plot of $\ln(R)$, where R is the resistance of the device, versus $1/T$, which shows good Arrhenius behaviour. The Coulomb charging energy measured from the slope of the Arrhenius plot is 2.02 ± 0.07 kJ/mol. (b) Plot of the I/V curve for the 1,4-PDI-saturated hybrid device depicted in the inset, where the gold nanoelectrodes and the gold nanoparticles within the gap are highlighted in yellow. This device shows negligible change in conductivity with temperature.

comprised nanoparticles located between the gold nanoelectrodes (an SEM image is shown as an inset to Fig. 4(a)), highlighted in yellow, where the average diameter d of nanoparticles between the gold electrodes is 11.2 ± 0.4 nm and $\frac{s}{d} = 0.46 \pm 0.03$, where s is the average interparticle separation. This 1,4-PDI-bridged hybrid system shows a significant change in conductivity after saturating with 1,4-PDI (Figure 4(a)), indicating that the oligomers can bridge a ~ 5 nm gap. This device configuration shows a conductivity that depends significantly on temperature with an Arrhenius dependence (shown as an insert to Fig. 4(a)) where $\ln(R)$, where R is the low-voltage resistance of the hybrid device, varies linearly with $1/T$, with a slope of 2.02 ± 0.07 kJ/mol. As expected for a system consisting of nano-scale inter-gap nodes, the conductivity has a significant Coulomb charging energy contribution. The Coulomb charging energy is given by: $E_c = \frac{e^2}{4\pi\epsilon_0\epsilon d(1/2 + s/d)}$, where e is the charge on the electron, ϵ_0 is the permittivity of free space and ϵ is the dielectric constant taken to be 3.5 for 1,4-PDI.⁴⁴ This results in a calculated Coulomb charging energy of 1.7 ± 0.1 kJ/mol, in good agreement with experiment.

A second type of hybrid device was found as shown by the example in Figure 4(b), where the nanoparticles decorate one of the nanoelectrodes (highlighted in yellow in the image shown as an inset to Fig. 4(b)) to decrease the nanogap to 9.2 ± 0.3 nm. The resulting I/V curve for a 1,4-PDI saturated gap shown in Fig. 4(b) has a resistance that is close infinity for $|V| < 1.5$ V, which decreases drastically at higher voltages. This behaviour differs from the theoretical⁴⁵ and experimental⁴⁶ single-molecule conductivities of gold-bridged 1,4-PDI where the high-resistance region occurs for $|V| < 0.5$ V, in accord with the linkers between the nanoparticle in the device shown in Fig. 4(a) being oligomeric species, and not single molecules. The I/V curves also show a very weak temperature dependences consistent with the oligomer bridging two nanoelectrodes.

This work tests the postulate that the growth of 1,4-PDI–Au oligomers nucleated by gold nanoparticles is inherently self-limiting because both the nucleation and growth occur at the peripheries of the nanoparticles so that the eventual saturation of the edge sites on the gold nanoparticles by oligomers prevent them from growing, inherently leading to self-limiting growth.⁴ Monte Carlo simulations of this process using the kinetic parameters previously found for oligomerization on a Au(111) substrate estimated that the maximum gap between gold nanoparticles that could be bridged by oligomers was ~ 10 nm.⁴ This postulate was tested on relatively large nanoparticle arrays, discrete nanogaps of ~ 30 nm, and hybrid devices consisting of thin gold films evaporated onto gold nanogap devices that all produced data that were consistent with this proposal; a nanogap of ~ 30 nm showed no conductivity when dosed with 1,4-PDI, while hybrid devices for which the interparticle separations were ~ 5 and 10 nm showed a significant increase in conductivity. It should be emphasized that, while there are currently no direct structural measurements of gold-containing oligomers between nanoparticles on silica, such linkages have been directly observed by STM on Au(111),⁹ a combination of conductivity measurements on gold nanoparticle arrays on silica and mica and measurements on hybrid devices allow a preliminary conclusions to be drawn that this approach provides a strategy for fabricating molecular-electronic circuits by judiciously changing the spacings between interconnecting gold nano-electrodes.

It was found that hybrid devices that contained discrete nanoparticles located within the gap showed an Arrhenius temperature dependence with an activation energy consistent with the calculated Coulomb charging energy, while the narrow gaps without inter-gap particles showed negligible temperature dependence. This suggests that even such simple molecular-electronic architectures can be used as molecular-electronic components. For example, devices containing nanoparticles within the gap (Fig. 4(a)) can be used as temperature sensors, while those with narrow gaps with strongly non-linear I/V curves (Fig. 4(b)) could find applications as voltage regulators where the regulation voltage can be adjusted by altering the oligomer length by changing the interelectrode separation.

Conflicts of interest

There are no conflicts to declare.

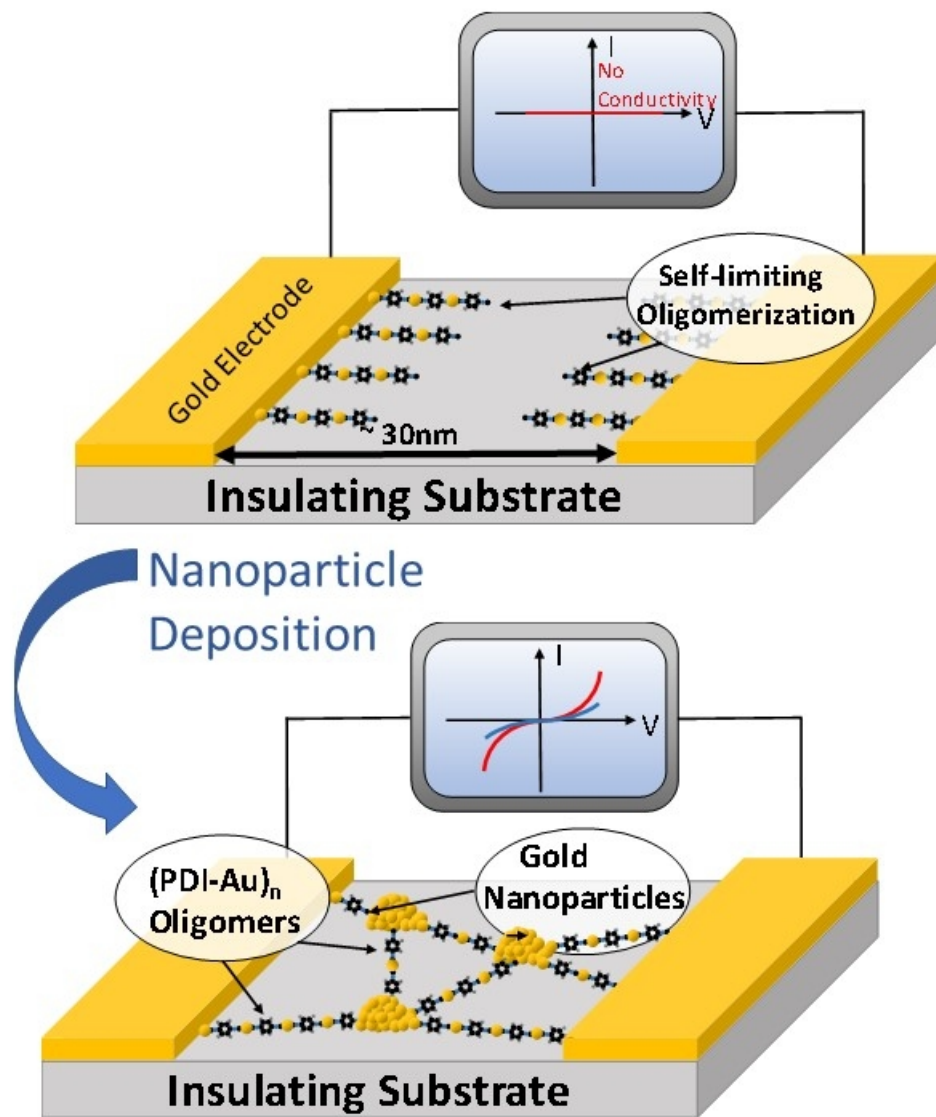
Notes and references

1. T. A. Gschneidtner, Y. A. Diaz Fernandez and K. Moth-Poulsen, *J. Mater. Chem. C*, 2013, **1**, 7127-7133.
2. A. Aviram and M. A. Ratner, *Chem. Phys. Lett.*, 1974, **29**, 277-283.
3. C. A. Mirkin and M. A. Ratner, *Annu. Rev. Phys. Chem.*, 1992, **43**, 719-754.
4. D. Olson, A. Boscoboinik, S. Manzi and W. T. Tysoe, *J. Phys. Chem. C*, 2019, **123**, 10398-10405.
5. A. M. Boscoboinik, S. J. Manzi, W. T. Tysoe, V. D. Pereyra and J. A. Boscoboinik, *Chem. Mater.*, 2015, **27**, 6642-6649.
6. J. Boscoboinik, J. Kestell, M. Garvey, M. Weinert and W. Tysoe, *Top. Catal.*, 2011, **54**, 20-25.
7. J. A. Boscoboinik, F. C. Calaza, Z. Habeeb, D. W. Bennett, D. J. Stacchiola, M. A. Purino and W. T. Tysoe, *Phys. Chem. Chem. Phys.*, 2010, **12**, 11624-11629.
8. J. Zhou, D. Acharya, N. Camillone, P. Sutter and M. G. White, *J. Phys. Chem. C*, 2011, **115**, 21151-21160.
9. J. Kestell, R. Abuflaha, J. A. Boscoboinik, Y. Bai, D. W. Bennett and W. T. Tysoe, *Chem Commun*, 2013, **49**, 1422-1424.
10. J. Kestell, R. Abuflaha, J. A. Boscoboinik, M. Garvey, D. W. Bennett and W. T. Tysoe, *J. Phys. Chem. Lett.*, 2014, **5**, 3577-3581.
11. M. Garvey, J. Kestell, R. Abuflaha, D. W. Bennett, G. Henkelman and W. T. Tysoe, *J. Phys. Chem. C*, 2014, **118**, 20899-20907.
12. R. Abuflaha, D. Olson, D. W. Bennett and W. T. Tysoe, *Surf. Sci.*, 2016, **649**, 56-59.
13. M. J. Robertson and R. J. Angelici, *Langmuir*, 1994, **10**, 1488-1492.
14. K.-C. Shih and R. J. Angelici, *Langmuir*, 1995, **11**, 2539-2546.
15. R. Abuflaha and W. T. Tysoe, *Appl. Phys. A-Mater*, 2018, **124**, 784.
16. M. Ito, H. Noguchi, K. Ikeda and K. Uosaki, *Phys. Chem. Chem. Phys.*, 2010, **12**, 3156-3163.
17. Kim, J. M. Beebe, Y. Jun, X. Y. Zhu and C. D. Frisbie, *J. Am. Chem. Soc.*, 2006, **128**, 4970-4971.
18. Y. Li, D. Lu, S. A. Swanson, J. C. Scott and G. Galli, *J. Phys. Chem. C*, 2008, **112**, 6413-6421.
19. K. L. Murphy, W. T. Tysoe and D. W. Bennett, *Langmuir*, 2004, **20**, 1732-1738.

COMMUNICATION

ChemComm

20. J. I. Henderson, S. Feng, G. M. Ferrence, T. Bein and C. P. Kubiak, *Inorg. Chim. Acta*, 1996, **242**, 115-124.
21. M. A. Reed, C. Zhou, C. J. Muller, T. P. Burgin and J. M. Tour, *Science*, 1997, **278**, 252-254.
22. S. N. Yaliraki, M. Kemp and M. A. Ratner, *J. Am. Chem. Soc.*, 1999, **121**, 3428-3434.
23. X. D. Cui, A. Primak, X. Zarate, J. Tomfohr, O. F. Sankey, A. L. Moore, T. A. Moore, D. Gust, G. Harris and S. M. Lindsay, *Science*, 2001, **294**, 571-574.
24. Y. Q. Xue and M. A. Ratner, *Phys. Rev. B*, 2003, **68**.
25. Xiao, Xu and N. J. Tao, *Nano Lett.*, 2004, **4**, 267-271.
26. M. Kiguchi, S. Miura, K. Hara, M. Sawamura and K. Murakoshi, *Appl. Phys. Lett.*, 2006, **89**.
27. R. B. Pontes, F. D. Novaes, A. Fazio and A. J. R. da Silva, *J. Am. Chem. Soc.*, 2006, **128**, 8996-8997.
28. M. Tsutsui, Y. Teramae, S. Kurokawa and A. Sakai, *Appl. Phys. Lett.*, 2006, **89**, 163111.
29. A. Arnold, F. Weigend and F. Evers, *J. Chem. Phys.*, 2007, **126**, 174101.
30. S. Yeganeh, M. A. Ratner, M. Galperin and A. Nitzan, *Nano Lett.*, 2009, **9**, 1770-1774.
31. K. Horiguchi, M. Tsutsui, S. Kurokawa and A. Sakai, *Nanotechnology*, 2009, **20**, 025204.
32. A. Mishchenko, D. Vonlanthen, V. Meded, M. Bürkle, C. Li, I. V. Pobelov, A. Bagrets, J. K. Viljas, F. Pauly, F. Evers, M. Mayor and T. Wandlowski, *Nano Lett.*, 2010, **10**, 156-163.
33. Y. Kim, T. Pietsch, A. Erbe, W. Belzig and E. Scheer, *Nano Lett.*, 2011, **11**, 3734-3738.
34. R. B. Pontes, A. R. Rocha, S. Sanvito, A. Fazio and A. J. R. da Silva, *ACS Nano*, 2011, **5**, 795-804.
35. I. Amlani, A. M. Rawlett, L. A. Nagahara and R. K. Tsui, *Appl. Phys. Lett.*, 2002, **80**, 2761-2763.
36. J. Kestell, R. Abuflaha, M. Garvey and W. T. Tysoe, *J. Phys. Chem. C*, 2015, **119**, 23042-23051.
37. P. Sheng, B. Abeles and Y. Arie, *Phys. Rev. Lett.*, 1973, **31**, 44-47.
38. B. Abeles, P. Sheng, M. D. Coutts and Y. Arie, *Adv. Phys.*, 1975, **24**, 407-461.
39. P. Sheng and J. Klafter, *Phys. Rev. B*, 1983, **27**, 2583-2586.
40. C. J. Adkins, *J. Phys.- Condens. Mat.*, 1989, **1**, 1253.
41. J. Herrmann, D. J. Bray, K. H. Müller, G. Wei and L. F. Lindoy, *Phys. Rev. B*, 2007, **76**, 212201.
42. S. Y. Quek, H. J. Choi, S. G. Louie and J. B. Neaton, *Nano Lett.*, 2009, **9**, 3949-3953.
43. L. Luo and C. D. Frisbie, *J. Am. Chem. Soc.*, 2010, **132**, 8854-8855.
44. J. Chen, L. C. Calvet, M. A. Reed, D. W. Carr, D. S. Grubisha and D. W. Bennett, *Chem. Phys. Lett.*, 1999, **313**, 741-748.
45. X. W. Yan, R. J. Liu, Z. L. Li, B. Zou, X. N. Song and C. K. Wang, *Chem. Phys. Lett.*, 2006, **429**, 225-228.
46. J.-O. Lee, G. Lientschnig, F. Wiertz, M. Struijk, R. A. J. Janssen, R. Egberink, D. N. Reinhoudt, P. Hadley and C. Dekker, *Nano Lett.*, 2003, **3**, 113-117.



165x190mm (96 x 96 DPI)